# Influence of vortex cooling and process parameters on the geometric characteristics of WAAM walls

***Nina Mucić*[1], *Jure Krolo*[1] *and Sonja Jozić*[1]**

*1) University of Split, Faculty of Electrical Engineering, Mechanical Engineering and Naval Architecture, Ruđera Boškovića 32, 21000 Split, Croatia*

*Corresponding author: Nina.Mucic.00@fesb.hr*

*Original scientific article*

**Abstract:** Wire arc additive manufacturing (WAAM) enables the production of metal components with high productivity and efficient material utilization. This study investigated the effects of wire feed speed (WFS), travel speed (TS), and active Vortex cooling time on the thermal cycle and geometric characteristics of aluminum alloy WAAM walls. The Taguchi method combined with Grey Relational Analysis (GRA) was applied for the multi-response optimization of the process parameters. The results showed that active Vortex cooling effectively reduces heat accumulation, while wire feed speed had the greatest influence on the overall assessment of the analyzed geometric characteristics. The optimal combination of process parameters was determined, contributing to a reduction in interpass temperature and improvements in geometric characteristics and material utilization during the WAAM process.

**Keywords:** *wire arc additive manufacturing (WAAM); vortex cooling; Taguchi method; Grey Relational Analysis (GRA)*

## 1. Introduction

Welding is one of the fundamental manufacturing technologies of modern industry and plays a key role in the production of metal structures and components of various sizes and applications. The development of welding processes, together with advances in automation, robotics, and digital manufacturing systems, has enabled the emergence of new manufacturing technologies that combine the advantages of arc welding and additive manufacturing. In recent decades, metal additive manufacturing has experienced significant growth due to its ability to produce complex geometries, reduce material waste, provide greater design freedom, and fabricate components using a layer-by-layer approach, making it an efficient alternative to conventional manufacturing processes in many applications. Among the various metal additive manufacturing technologies, Wire Arc Additive Manufacturing (WAAM) has attracted considerable attention as a Directed Energy Deposition (DED) process. In the WAAM process, an electric arc serves as the heat source, while a metal wire is continuously fed as the feedstock material and deposited layer by layer along a predefined toolpath. Compared with technologies that use metal powder as the feedstock material, WAAM is characterized by a significantly higher material deposition rate, lower raw material and equipment costs, and high material utilization, making it particularly suitable for the production of medium- and large-scale near-net-shape metal components [1]. By using wire as the feedstock material, WAAM achieves nearly complete material utilization and, compared with processes employing metal powder, provides simpler feedstock handling and lower manufacturing costs [2]. Owing to these advantages, interest in the application of this technology has grown steadily in recent years across both industry and the scientific community, particularly in the aerospace, shipbuilding, energy, and other industrial sectors [3]. Among the various groups of materials used in the WAAM process, aluminum alloys occupy a prominent position due to their low density, high strength-to-weight ratio, good corrosion resistance, and widespread use in the aerospace, automotive, marine, and transportation industries. However, their high thermal conductivity, pronounced tendency to form an oxide layer, susceptibility to porosity formation, and the occurrence of thermal distortion during multilayer deposition make the production

of high-quality aluminum WAAM components a significant technological challenge [3]. For this reason, considerable research efforts in recent years have focused on the development of aluminum alloys tailored for the WAAM process, as well as on the optimization of process parameters and the thermal cycle during fabrication. The final quality of WAAM components is strongly influenced by the selected process parameters, the thermal cycle, and the heat management strategy employed during the process [4]. One of the major challenges in WAAM is heat accumulation, which results from the successive deposition of layers, preventing previously deposited layers from cooling completely before the next layer is applied. An increase in the interpass temperature alters the thermal cycle and may lead to changes in wall geometry, reduced geometric accuracy, the development of a heterogeneous microstructure, porosity formation, residual stresses, and variations in the mechanical properties of the fabricated components. At the same time, the temperature increase during multilayer deposition adversely affects process repeatability and makes it more difficult to maintain stable geometry when fabricating taller walls [2], [5]–[7].

Consequently, significant attention has recently been directed toward the development of various thermal management strategies for the WAAM process. The objective of active cooling is not only to reduce heat accumulation but also to maintain a stable interpass temperature, increase productivity by reducing the waiting time between successive layers, and achieve more uniform geometry and more homogeneous properties of the fabricated components. For example, Heinrich et al. demonstrated that active substrate cooling can reduce the required waiting time between successive layers by up to 50%, while the post-process cooling time of the component can be shortened by up to 75%, without compromising the quality of the fabricated components [8]. Various thermal management approaches have been proposed in the literature, including increasing the interpass time, substrate cooling, compressed air cooling, carbon dioxide cooling, water cooling, and other active cooling systems aimed at improving process stability [5], [7]–[9]. Although several active cooling methods, such as shielding gas cooling, thermoelectric cooling, and reduced heat input, have been proposed, some of these approaches exhibit limitations in terms of efficiency or adaptability to different WAAM systems [5], [10].

In this study, the application of a Vortex tube as an alternative active cooling method for the WAAM process was investigated. A Vortex tube operates based on the Ranque–Hilsch effect, separating compressed air into hot and cold air streams without the use of moving parts or additional refrigerants [11]. Previous studies have shown that Vortex cooling can effectively reduce interpass temperature and heat accumulation, improve the geometric accuracy of fabricated walls, reduce porosity, and promote the formation of a finer microstructure and improved mechanical properties [10]. Although numerous studies have demonstrated that different active cooling methods can significantly influence the thermal cycle of the WAAM process, their effects on the geometric characteristics of fabricated components still require further investigation, particularly when the interaction of multiple process parameters and their multi-response optimization are considered simultaneously [5], [7] and [9]. Therefore, further research is needed to clarify the relationship between the thermal cycle, geometric characteristics, and process parameter optimization in the WAAM process [12]. Accordingly, the aim of this study was to investigate the effects of Vortex cooling time, wire feed speed (*WFS*), and travel speed (*TS*) on the geometric characteristics of aluminum alloy WAAM walls. In addition to thermal cycle analysis, a geometric characterization of the fabricated walls was performed, and the Taguchi method combined with Grey Relational Analysis (GRA) was applied to determine the optimal combination of process parameters.

## 2. Materials and Methods

The experimental part of the study was conducted using the Wire Arc Additive Manufacturing (WAAM) process. Aluminum alloy EN AW-1050A plates with dimensions of 100 × 200 × 4 mm were used as the substrate material due to their high thermal conductivity, which enables efficient heat dissipation during the WAAM process, good weldability, and cost-effectiveness [13]. A solid ER2319 aluminum wire was used as the feedstock material. This filler material was primarily developed for welding Al–

Cu aluminum alloys, providing high weld strength, good ductility, and improved resistance to stress corrosion cracking. Its chemical composition is characterized by an increased copper content (5.80–6.80%), together with controlled amounts of manganese (0.20–0.40%), titanium (0.10–0.20%), zirconium (0.10–0.25%), and vanadium (0.05–0.15%), while the contents of silicon, iron, zinc, and magnesium are limited to very low levels. This chemical composition contributes to stable metal transfer during the process, good resistance to hot cracking, and favorable mechanical properties after solidification [14]. The selected combination of the substrate and feedstock materials was based on their good weldability, process stability, and widespread application in studies of aluminum welded joints and WAAM technology.

The specimens were fabricated using a robotic cell centered around a six-axis ABB IRB 1600-6/1.45 industrial robot. The ABB IRB 1600 robot series was developed for demanding welding applications in which path accuracy and motion stability are essential for achieving high-quality welded joints [15], [16]. The robot was controlled by an ABB IRC5 controller, which serves as the central control unit of the robotic cell. A Fronius TPS 4000i power source was used for the experiments, providing synergic control of the welding parameters and stable feedstock transfer throughout the process. To reduce heat accumulation during multilayer WAAM fabrication, a Vortec Cold Air Gun Model 610 active cooling system was integrated into the experimental setup. The cold air stream was directed toward the deposition area to enhance heat dissipation during the fabrication of the WAAM walls. A Fini BK119-270L reciprocating air compressor, with a rated power of 5.5 kW and a maximum operating pressure of 10 bar, was used to supply compressed air to the Vortex cooling system.

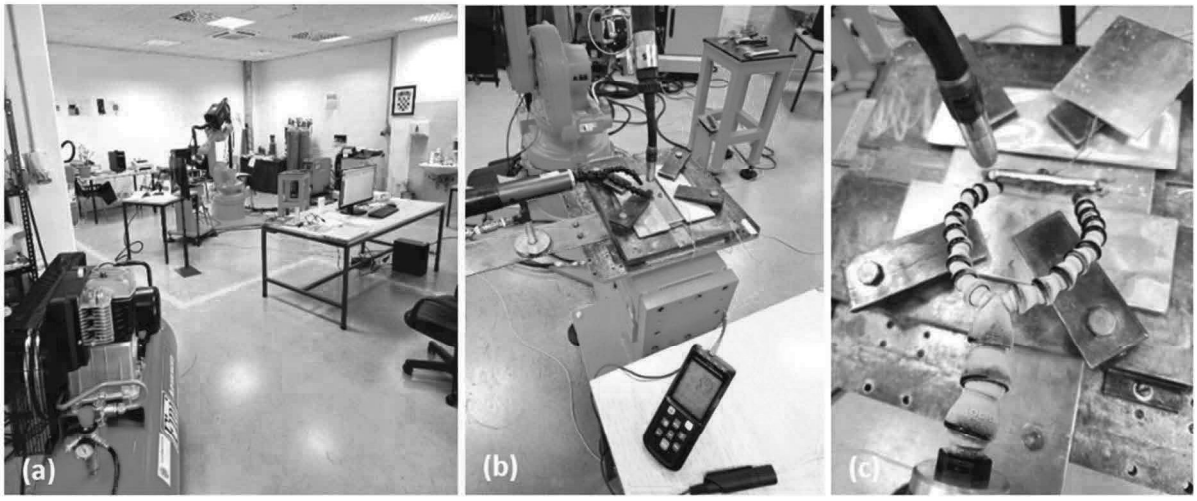



***Figure 1.*** *Experimental setup used during the WAAM process: (a) overview of the robotic cell, (b) position of the infrared thermometer during the experiment, and (c) Vortex active cooling system*

The experimental design was established using the Taguchi L9 orthogonal array, enabling a systematic investigation of the effects of the process parameters while reducing the number of required experiments. During the study, the wire feed speed (*WFS*), travel speed (*TS*), and Vortex cooling time were varied, whereas all other process parameters were kept constant to enable an isolated analysis of their effects on the geometric characteristics of the fabricated specimens. The combinations of the process parameters used in the experimental design are presented in Table 1. Prior to the main experimental campaign, preliminary tests were conducted to determine the appropriate ranges of the process parameters. Based on the obtained results, the Vortex cooling time was selected in the range of 0–120 s, the wire feed speed (*WFS*) in the range of 8–16 m/min, and the travel speed (*TS*) in the range of 6–7 mm/s. After defining the experimental design, the robot program was developed using the RobotStudio software package and subsequently transferred to the robotic cell. Following program transfer, the welding process was carried out to fabricate the specimens. Based on the obtained results, a wall length of 100 mm was selected.

***Table 1.*** *Experimental design based on the Taguchi L9 orthogonal array*

| Run | A: Vortex cooling time (s) | B: Wire feed speed (*WFS*) (m/min) | C: Travel speed (*TS*) (mm/s) |
|---|---|---|---|
| 1 | 0.00 | 8.00 | 6.00 |
| 2 | 0.00 | 12.00 | 6.50 |
| 3 | 0.00 | 16.00 | 7.00 |
| 4 | 60.00 | 8.00 | 6.50 |
| 5 | 60.00 | 12.00 | 7.00 |
| 6 | 60.00 | 16.00 | 6.00 |
| 7 | 120.00 | 8.00 | 7.00 |
| 8 | 120.00 | 12.00 | 6.00 |
| 9 | 120.00 | 16.00 | 6.50 |

The deposited wall was positioned centrally on the substrate plate measuring 100 × 200 mm, with the start and end points located 50 mm from the plate edges. A total of nine specimens were fabricated, each using a different combination of process parameters. Each specimen consisted of eight successive layers, while the waiting time between two consecutive layers was set to 120 s. This approach enabled partial cooling of the previously deposited layer before the deposition of the subsequent layer and ensured consistent thermal regime during the fabrication of all specimens. To determine the cross-sectional geometry of the fabricated walls, the specimens were prepared for metallographic analysis. Each wall was sectioned into three equally spaced cross-sections, resulting in a total of 27 cross-sections for further analysis. Sectioning was performed using a Buehler Delta AbrasiMet metallographic cut-off machine. Grinding was carried out on a Struers LaboPol-2 grinding machine equipped with an automatic LaboForce-3 polishing head using P1200 grinding paper. The geometric analysis of the cross-sections was performed using an Olympus SZ61 stereomicroscope equipped with a ToupTek E3ISPM08300KPB digital microscope camera, while image acquisition was carried out using the ToupView software package. Representative cross-sections of all fabricated WAAM specimens are presented in Figure 2, illustrating the effect of the different process parameter combinations listed in Table 1 on the wall geometry.

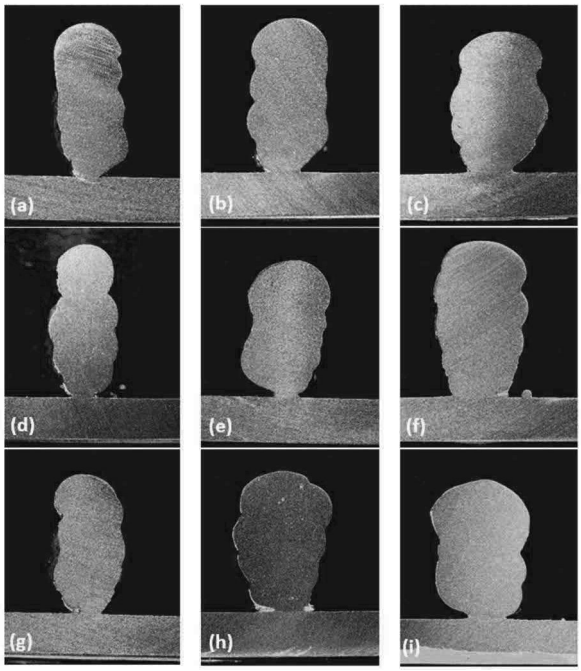



***Figure 2.*** *Cross-sections of the WAAM specimens fabricated using the process parameter combinations listed in Table 1 (a–i)*

The geometric characteristics were analyzed using ImageJ software. After calibration, the maximum wall width (*MWW*), effective wall width (*EWW*), effective usable wall area (*EUWA*), total cross-sectional area ($A_{tot}$), maximum wall height ($H_{max}$), and the characteristic dimensions *a* and *b* were determined (Figure 3). Based on these measurements, the surface irregularity index (*SI*) and material utilization (*MU*) were calculated to evaluate the material deposition efficiency for different process parameter combinations. These parameters are defined as follows:

$$SI = \frac{(MWW - EWW)}{2} \tag{1}$$

$$MU = \frac{EUWA}{(EUWA + a + b)} \tag{2}$$

In addition to the geometric analysis, the thermal cycle of the process was analyzed using a TC 319 contact thermometer. The temperature was continuously measured at the central region of the substrate plate, adjacent to the weld bead, enabling continuous monitoring of the thermal cycle during specimen fabrication. Based on the recorded temperature curves, the interpass temperature immediately before the deposition of each layer ($T_{interpass}$), the maximum temperature reached during layer deposition ($T_{max}$), and the interpass temperature immediately before the deposition of the subsequent layer ($T_{interpass\ next}$) were determined. The cooling temperature difference (Cooling Δ*T*) was calculated as the difference between $T_{max}$ and $T_{interpass\ next}$, while the average cooling rate (Cooling Rate) was calculated as the ratio of Cooling Δ*T* to the corresponding cooling time ($t_{cool}$), as defined by Equations (3) and (4).

$$\text{Cooling } \Delta\text{T} = Tmax\ -\ T\ interpass\ next \tag{3}$$

$$Cooling\ Rate\ = \frac{\text{Cooling } \Delta\text{T}}{t\ cool} \tag{4}$$

For each of the nine experiments, the Fronius Xplorer software generated diagrams of the welding current, arc voltage, and wire feed speed. These data served as the basis for the analysis of the thermal cycle and the geometric characteristics of the fabricated WAAM walls presented in the following section.

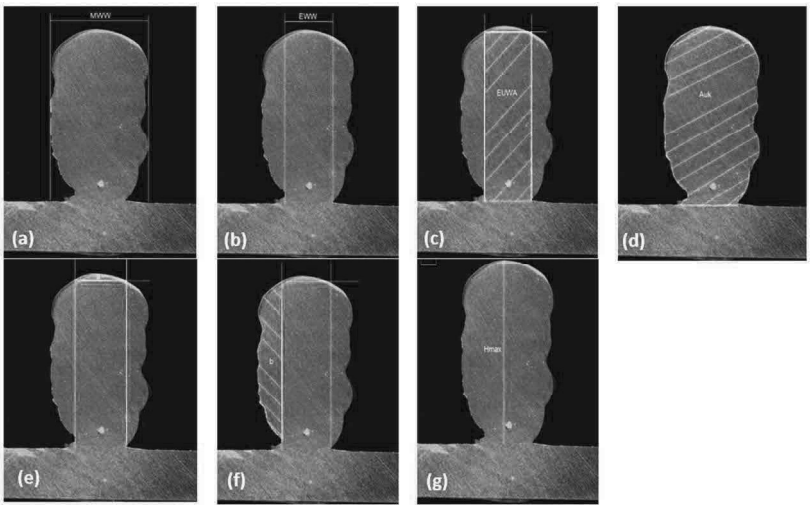



***Figure 3.*** *Cross-sectional geometric characteristics determined in ImageJ for specimen 6: (a) maximum wall width (MWW), (b) effective wall width (EWW), (c) effective usable wall area (EUWA), (d) total cross-sectional area ($A_{tot}$), (e) characteristic dimension a, (f) characteristic dimension b, and (g) maximum wall height ($H_{max}$)*

## 3. Results and Discussion

This section presents an analysis of the influence of the process parameters on the thermal cycle and the geometric characteristics of the WAAM walls. The results are presented through the analysis of thermal indicators and geometric parameters to determine their relationship and their influence on process stability.

### 3.1. Effect of Vortex Cooling on the Thermal Cycle of the WAAM Process

To analyze the effect of Vortex cooling on the thermal cycle, the average thermal indicators, namely average interpass temperature, average cooling rate, and average maximum temperature, are presented in Figure 4. Since the optimization in this study was performed based on the geometric characteristics of the WAAM walls, specimens 3, 6, and 7 from Table 1, corresponding to Vortex cooling times of 0 s, 60 s, and 120 s, respectively, were selected for a more detailed analysis of the thermal cycles. Although the selected runs correspond to different Vortex cooling times, they also differ in wire feed speed and/or travel speed. Therefore, the presented thermal cycles illustrate the combined response of the selected process conditions and should not be interpreted as the isolated effect of cooling time. Although the selected runs do not allow the isolated influence of Vortex cooling to be quantified, they provide a representative illustration of the thermal trends observed under the investigated processing conditions. Their representative temperature cycles are presented in Figure 5 to compare the effect of different Vortex cooling times on the development of the thermal cycle, while a more detailed analysis of the thermal indicators will be the subject of future research.

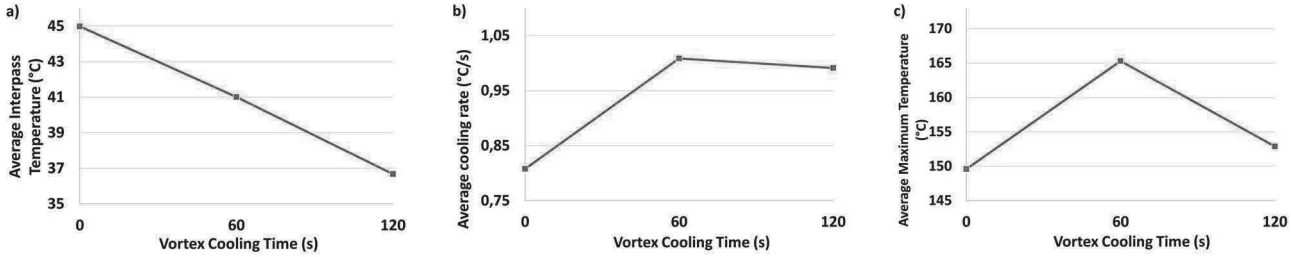



***Figure 4.*** *Effect of Vortex cooling time on the average thermal indicators of the WAAM process: a) average interpass temperature, b) average cooling rate, and c) average maximum temperature*

As the Vortex cooling time increased from 0 to 120 s, a continuous decrease in the average interpass temperature was observed, from 44.98 °C to 36.67 °C, corresponding to a reduction of approximately 18.5% (Figure 4a). At the same time, the average cooling rate increased from 0.808 °C/s to 1.008 °C/s at a cooling time of 60 s, while a very similar value of 0.991 °C/s was recorded at 120 s (Figure 4b). This trend confirms that active Vortex cooling effectively limits heat accumulation between successive passes and provides a more stable thermal regime during the WAAM process, which is consistent with the findings reported by Wang et al. [10], Heinrich et al. [8], and Rodrigues et al. [3].

Unlike the average interpass temperature and average cooling rate, the average maximum temperature did not exhibit a consistent trend (Figure 4c). This can be explained by the fact that the maximum temperature depends not only on the Vortex cooling time but also on the combination of process parameters defined by the Taguchi experimental design. An increase in the wire feed speed (WFS) results in a higher heat input into the process, thereby affecting the maximum temperature achieved. Similar observations were reported by Wu et al. [2] and Rodrigues et al. [3], who emphasized that the interpass temperature is a more reliable indicator of thermal cycle control than the maximum process temperature. The obtained results confirm that the Vortex cooling time is one of the key parameters for controlling the thermal cycle during the WAAM process. The reduction in the average interpass temperature accompanied by an increase in the average cooling rate indicates more efficient heat dissipation and reduced heat accumulation between successive passes, whereas extending the cooling time beyond 60 s provides only a limited improvement in the thermal indicators. This finding

is important for the optimization of the WAAM process, as it enables the selection of a cooling time that ensures stable thermal regime without unnecessarily increasing the overall fabrication time.

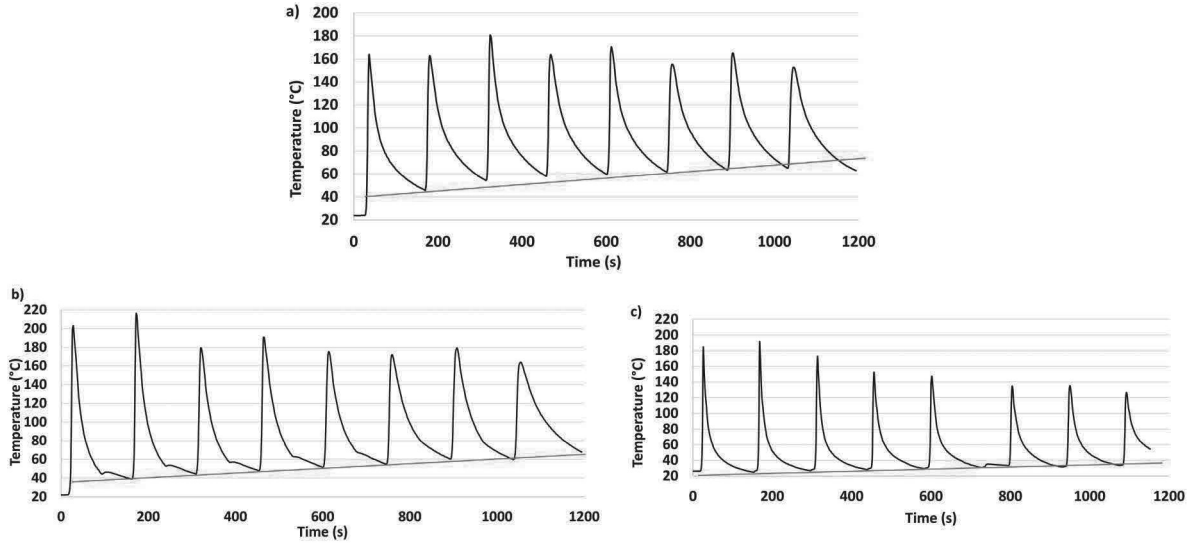



***Figure 5.*** *Representative temperature cycles of the selected experiments: a) Run 3 – without Vortex cooling, b) Run 6 – 60 s of Vortex cooling, and c) Run 7 – 120 s of Vortex cooling*

Figure 5 shows the representative temperature cycles of the selected experiments, Run 3, Run 6, and Run 7, corresponding to Vortex cooling times of 0, 60, and 120 s, respectively. The red trend lines illustrate the evolution of the interpass temperature during the fabrication of the WAAM walls. Without the application of Vortex cooling, the interpass temperature increased progressively from pass to pass, indicating pronounced heat accumulation in the substrate plate and the deposited wall. With 60 s of Vortex cooling, the increase in interpass temperature was considerably less pronounced, whereas with 120 s of cooling, the interpass temperature returned to approximately the same value before each subsequent pass, indicating a more stable thermal regime and more efficient heat dissipation. As the Vortex cooling time increased, heat accumulation in the substrate plate decreased, while the overall shape of the temperature cycles remained nearly unchanged. These results confirm that Vortex cooling primarily reduces heat accumulation and contributes to a more stable thermal regime during the WAAM process, which is consistent with the findings reported by Rodrigues et al. [3] and Wang et al. [10].

### 3.2. Effect of Wire Feed Speed on the Electrical Process Parameters

To analyze the effect of wire feed speed on the electrical process parameters of the WAAM process, representative current and voltage waveforms recorded during the final pass are presented in Figure 6 for experiments Run 1, Run 2, and Run 3, corresponding to wire feed speeds of 8, 12, and 16 m/min, respectively.

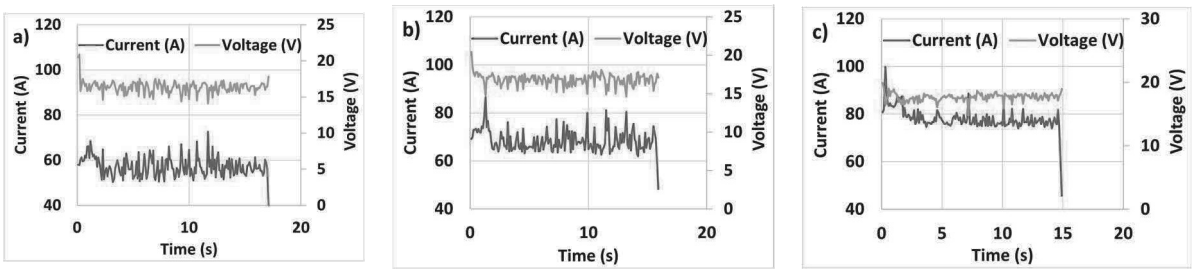



***Figure 6.*** *Effect of wire feed speed on the current and voltage waveforms during the final pass of the WAAM process: a) WFS = 8 m/min, b) WFS = 12 m/min, and c) WFS = 16 m/min*

Under all investigated conditions, after the initial arc ignition, the process reached a stable state, with the electrical parameters exhibiting relatively small fluctuations during deposition. At the end of each pass, a decrease in the welding current was observed, corresponding to arc extinction after the completion of welding. The analysis of the average electrical parameters revealed a clear influence of wire feed speed on the welding current. At *WFS* = 8 m/min, the average welding current was 57.15 A, increasing to 68.36 A at *WFS* = 12 m/min and 77.94 A at *WFS* = 16 m/min. At the same time, the average arc voltage was 16.35 V, 16.83 V, and 17.66 V, respectively. The results of the electrical parameter analysis are consistent with the previously presented geometric characteristics of the fabricated WAAM walls.

## 4. Multi-Objective Optimization of Process Parameters

The objective of the multi-objective optimization is to determine the optimal combination of process parameters that simultaneously provides the most favourable values of all considered process responses. To determine the optimal combination of process parameters, multi-objective optimization was performed using the Taguchi method combined with Grey Relational Analysis (GRA). This approach enables the integration of multiple process responses into a single quality indicator, namely the Grey Relational Grade (GRG), thereby simplifying the ranking of the experimental runs and the determination of the optimal levels of the process parameters. Four geometric characteristics of the fabricated WAAM walls were included in the optimization: material utilization (*MU*), surface irregularity index (*SI*), effective usable wall area (*EUWA*), and maximum wall height ($H_{max}$). The input process parameters considered were Vortex cooling time (s), wire feed speed (WFS) (m/min), and travel speed (*TS*) (mm/s). Since no geometric characteristic was assigned greater importance than the others, equal weights were assigned to all analyzed responses, and the final Grey Relational Grade was calculated as the arithmetic mean of the grey relational coefficients.

***Table 2.*** *Average values of the output geometric characteristics used for the multi-objective optimization*

| Run | Average *MU* | Average *SI* (mm) | Average *EUWA* ($mm^2$) | Average $H_{max}$ (mm) |
|---|---|---|---|---|
| 1 | 0.542 | 2.858 | 24.584 | 13.904 |
| 2 | 0.635 | 2.510 | 32.159 | 12.962 |
| 3 | 0.729 | 2.661 | 46.191 | 13.211 |
| 4 | 0.616 | 2.151 | 30.346 | 13.427 |
| 5 | 0.558 | 2.500 | 29.338 | 12.396 |
| 6 | 0.759 | 1.990 | 60.469 | 13.864 |
| 7 | 0.513 | 2.354 | 23.437 | 12.271 |
| 8 | 0.559 | 2.901 | 34.203 | 13.007 |
| 9 | 0.673 | 2.259 | 46.565 | 12.730 |

The average values of the geometric characteristics used for the multi-objective optimization are presented in Table 2. For each experimental run, the values of the input process parameters together with the corresponding average values of material utilization (*MU*), surface irregularity index (*SI*), effective usable wall area (*EUWA*), and maximum wall height ($H_{max}$) are presented. These data constitute the basis for the Grey Relational Analysis (GRA) and the calculation of the Grey Relational Grades (GRGs).

***Table 3.*** *Normalized values of the geometric characteristics*

| RUN | *MU* | *SI* | *EUWA* | $H_{max}$ |
|---|---|---|---|---|
| 1 | 0.119 | 0.047 | 0.031 | 1.000 |
| 2 | 0.496 | 0.429 | 0.236 | 0.423 |
| 3 | 0.878 | 0.263 | 0.614 | 0.576 |
| 4 | 0.421 | 0.823 | 0.187 | 0.708 |
| 5 | 0.182 | 0.440 | 0.159 | 0.077 |
| 6 | 1.000 | 1.000 | 1.000 | 0.976 |
| 7 | 0.000 | 0.600 | 0.000 | 0.000 |
| 8 | 0.189 | 0.000 | 0.291 | 0.451 |
| 9 | 0.651 | 0.705 | 0.625 | 0.281 |

Normalization was performed to transform all process responses onto a common dimensionless scale ranging from 0 to 1, thereby enabling their direct comparison. The larger-the-better criterion was applied to the geometric characteristics *MU*, *EUWA*, and $H_{max}$, whereas the smaller-the-better criterion was applied to the surface irregularity index (SI), for which lower values are desirable.

***Table 4.*** *Grey Relational Coefficients (GRCs) for the analyzed geometric characteristics*

| RUN | *MU* | *SI* | *EUWA* | $H_{max}$ |
|---|---|---|---|---|
| 1 | 0.362 | 0.344 | 0.340 | 1.000 |
| 2 | 0.498 | 0.467 | 0.395 | 0.464 |
| 3 | 0.803 | 0.404 | 0.565 | 0.541 |
| 4 | 0.464 | 0.739 | 0.381 | 0.631 |
| 5 | 0.379 | 0.472 | 0.373 | 0.351 |
| 6 | 1.000 | 1.000 | 1.000 | 0.953 |
| 7 | 0.333 | 0.556 | 0.333 | 0.333 |
| 8 | 0.381 | 0.333 | 0.413 | 0.477 |
| 9 | 0.589 | 0.629 | 0.571 | 0.410 |

Based on the normalized values, the Grey Relational Coefficients (GRCs) were calculated to quantify the closeness of each process response to the ideal solution. Higher GRC values indicate smaller deviations from the reference sequence and, consequently, more favourable values of the considered geometric characteristics. The calculated Grey Relational Coefficients were then used to determine the final Grey Relational Grade (GRG), which represents a single indicator of the overall quality of each experimental run.

***Table 5.*** *Grey Relational Grades (GRGs) and ranking of the experimental runs*

| RUN | *Γ* | Rank |
|---|---|---|
| 1 | 0.512 | 5 |
| 2 | 0.456 | 6 |
| 3 | 0.578 | 2 |
| 4 | 0.554 | 3 |
| 5 | 0.394 | 8 |
| 6 | 0.988 | 1 |
| 7 | 0.389 | 9 |
| 8 | 0.401 | 7 |
| 9 | 0.550 | 4 |

The Grey Relational Grades (GRGs) and the corresponding rankings of the experimental runs are presented in Table 5. A higher GRG value indicates a closer proximity to the ideal solution and, consequently, a more favourable compromise among all analyzed geometric characteristics. As shown in Table 5, experimental run 6 achieved the highest GRG value ($\Gamma$ = 0.988), indicating that this combination of process parameters resulted in the highest overall quality of the fabricated WAAM walls. In contrast, the lowest GRG value was recorded for experimental run 7 ($\Gamma$ = 0.389), indicating

the least favourable combination of process parameters within the analyzed experimental domain. These results confirm that Grey Relational Analysis enables the integration of multiple geometric characteristics into a single quality indicator and provides a clear ranking of the experimental runs according to their overall performance.

***Table 6.*** *Effect of Process Parameters on the Grey Relational Grade (GRG)*

| Input Process Parameter | Level 1 | Level 2 | Level 3 | Max | Min | Δ | Rank |
|---|---|---|---|---|---|---|---|
| Vortex cooling time | 0.515 | 0.645 | 0.447 | 0.645 | 0.447 | 0.199 | 2 |
| Wire Feed Speed (*WFS*) | 0.485 | 0.417 | 0.705 | 0.705 | 0.417 | **0.288** | **1** |
| Travel Speed (*TS*) | 0.634 | 0.520 | 0.454 | 0.634 | 0.454 | 0.180 | 3 |

The average Grey Relational Grades (GRGs) at different levels of the process parameters are presented in Table 6. The largest difference between the maximum and minimum average GRG values (Δ = 0.288) was obtained for the wire feed speed (*WFS*), indicating that this process parameter has the greatest influence on the overall quality of the fabricated WAAM walls. It is followed by the Vortex cooling time (Δ = 0.199), while the smallest influence was observed for the travel speed (*TS*) (Δ = 0.180). These results indicate that the wire feed speed has the most pronounced effect on the analyzed geometric characteristics, whereas Vortex cooling time also contributes significantly to the overall process quality. The main effects plots of the process parameters on the Grey Relational Grade (GRG) are presented in Figure 7.

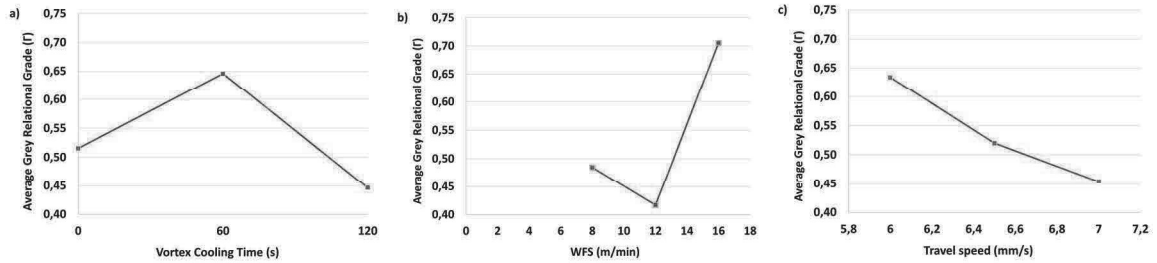



***Figure 7.*** *Main effects plots of the process parameters on the Grey Relational Grade (GRG): a) Vortex cooling time, b) wire feed speed (WFS), and c) travel speed (TS)*

As shown in the main effects plots, the highest average GRG values were obtained at Level 2 (60 s) for the Vortex cooling time, Level 3 (16 m/min) for the wire feed speed, and Level 1 (6 mm/s) for the travel speed. These results confirm the findings presented in Table 6 and indicate that the optimal combination of process parameters corresponds to $A_2B_3C_1$, i.e., a Vortex cooling time of 60 s, a wire feed speed of 16 m/min, and a travel speed of 6 mm/s. This combination provides the highest overall quality of the fabricated WAAM walls within the investigated experimental domain. The optimal combination can be attributed to the highest heat input achieved at the highest wire feed speed and the lowest travel speed, resulting in wider initial layers and an increased effective usable wall area (*EUWA*). Applying Vortex cooling for 60 s limits heat accumulation between successive passes, thereby improving the overall process performance. Future studies should evaluate the wall geometry after excluding the narrower initial layers to better distinguish the influence of the initial thermal regime from the effect of Vortex cooling on the geometric characteristics. The analysis of variance (ANOVA) for the Grey Relational Grade (GRG) is presented in Table 7.

***Table 7.*** *Analysis of Variance (ANOVA) for the Grey Relational Grade (GRG)*

| Source | DF | SS | MS | *F*-Value | *p*-Value | Contribution (%) |
|---|---|---|---|---|---|---|
| Vortex Time | 2 | 0.061 | 0.031 | 2.294 | 0.304 | 22.287 |
| WFS | 2 | 0.136 | 0.068 | 5.130 | 0.163 | 49.831 |
| TS | 2 | 0.050 | 0.025 | 1.870 | 0.348 | 18.168 |
| Error | 2 | 0.027 | 0.013 | | | 9.714 |
| Total | 8 | 0.274 | | | | 100.000 |

The results of the analysis of variance confirm the findings obtained from the Grey Relational Analysis and the main effects plots. The wire feed speed made the largest contribution to the overall variation of the Grey Relational Grade, confirming that this process parameter plays the dominant role in determining the overall quality of the fabricated WAAM walls. The Vortex cooling time exhibited the second-largest contribution, whereas the smallest contribution was observed for the travel speed. These results confirm that optimizing the geometric characteristics requires both an appropriate selection of the amount of deposited material and effective control of the process thermal cycle.

$$\hat{\Gamma} = \Gamma m + (\bar{\Gamma}A2 - \Gamma m) + (\bar{\Gamma}B3 - \Gamma m) + (\bar{\Gamma}C1 - \Gamma m) = 0.912 \quad (5)$$

In the Grey Relational Grade prediction equation, $\hat{\Gamma}$ is the predicted Grey Relational Grade (GRG), $\Gamma m$ is the overall mean GRG, and $\bar{\Gamma}A2$, $\bar{\Gamma}B3$, $\bar{\Gamma}C1$ are the mean GRG values at the optimal levels of Vortex cooling time, Wire Feed Speed, and Travel Speed, respectively. Based on equation 5, the predicted GRG for the optimal process parameter combination is 0.912. The predicted result is in agreement with the Grey Relational Analysis and confirms the effectiveness of the proposed optimization approach for selecting the optimal WAAM process parameters.

## 5. Conclusions

Based on the experimental investigation of the effects of process parameters on the thermal cycle and geometric characteristics of WAAM walls fabricated using active Vortex cooling, the following conclusions can be drawn:

- The application of Vortex cooling reduced the interpass temperature and heat accumulation during multi-layer WAAM fabrication. Increasing the Vortex cooling time from 0 to 120 s reduced the average interpass temperature by approximately 18.5%, contributing to a more stable thermal regime.
- The highest average cooling rate was achieved with a Vortex cooling time of 60 s. Extending the cooling time to 120 s primarily resulted in a further reduction of the interpass temperature, while the increase in the average cooling rate was negligible.
- The combination of the highest wire feed speed and the lowest travel speed produced the highest heat input among the analyzed experimental runs, resulting in wider initial layers. Nevertheless, applying Vortex cooling for 60 s effectively limited heat accumulation between successive passes while maintaining favourable geometric characteristics of the fabricated WAAM walls.
- The wire feed speed was identified as the most influential process parameter affecting the geometric characteristics of the fabricated WAAM walls. Increasing the wire feed speed (WFS) from 8 to 16 m/min increased the effective usable wall area (*EUWA*) by approximately 96%, while the material utilization (*MU*) increased by about 29%.
- The Grey Relational Grade (GRG), representing the overall evaluation of the analyzed geometric characteristics, was influenced predominantly by the wire feed speed (49.83%), followed by the Vortex cooling time (22.29%), whereas the travel speed had the smallest contribution (18.17%).

- The optimal combination of process parameters was identified as $A_2B_3C_1$, corresponding to a Vortex cooling time of 60 s, a wire feed speed of 16 m/min, and a travel speed of 6 mm/s, with a predicted Grey Relational Grade of Γ = 0.912.

## Acknowledgements

This work was supported by the European Union under the NextGenerationEU in-strument, through the Recovery and Resilience Mechanism, within the institutional research project AIMTECH 4.5 (IP-UNIST-07), implemented by the Ministry of Science, Education and Youth of the Republic of Croatia.

## References

[1] Williams, S.W., Martina, F., Addison, A.C., Ding, J., Pardal, G., Colegrove, P., 2016. Wire + Arc Additive Manufacturing. Materials Science and Technology, 32 (7), 641–647.

[2] Wu, B., Pan, Z., Ding, D., Cuiuri, D., Li, H., Xu, J., Norrish, J., 2018. A review of the wire arc additive manufacturing of metals: properties, defects and quality improvement. Journal of Manufacturing Processes, 35, 127–139.

[3] Rodrigues, T.A., Duarte, V., Miranda, R.M., Santos, T.G., Oliveira, J.P., 2019. Current Status and Perspectives on Wire and Arc Additive Manufacturing (WAAM). Materials, 12 (7), 1121.

[4] Langelandsvik, G., Akselsen, O.M., Furu, T., Roven, H.J., 2021. Review of Aluminum Alloy Development for Wire Arc Additive Manufacturing. Materials, 14 (18), 5370.

[5] Reindl, T., Rotzsche, S., Hempel, N., Mayr, P., 2026. Development and evaluation of an advanced wire-arc directed energy deposition process with integrated temperature control and in-situ heat treatment. Progress in Additive Manufacturing, 11, 2315–2329.

[6] Zhai, W., Wu, N., Zhou, W., 2022. Effect of Interpass Temperature on Wire Arc Additive Manufacturing Using High-Strength Metal-Cored Wire. Metals, 12 (2), 212.

[7] Scotti, F.M., Teixeira, F.R., da Silva, L.J., de Araújo, D.B., Reis, R.P., Scotti, A., 2020. Thermal management in WAAM through the CMT Advanced process and an active cooling technique. Journal of Manufacturing Processes, 57, 23–35.

[8] Heinrich, L., Feldhausen, T., Saleeby, K., Kurfess, T., Saldaña, C., 2023. Build plate conduction cooling for thermal management of wire arc additive manufactured components. The International Journal of Advanced Manufacturing Technology, 124 (5), 1557–1567.

[9] Wu, B., Pan, Z., Ding, D., Cuiuri, D., Li, H., Fei, Z., 2018. The effects of forced interpass cooling on the material properties of wire arc additively manufactured Ti6Al4V alloy. Journal of Materials Processing Technology, 258, 97–105.

[10] Wang, B., Yang, G., Zhou, S., Cui, C., Qin, L., 2020. Effects of On-Line Vortex Cooling on the Microstructure and Mechanical Properties of Wire Arc Additively Manufactured Al-Mg Alloy. Metals, 10 (8), 1004.

[11] Gao, C., 2005. Experimental Study on the Ranque-Hilsch Vortex Tube. PhD Thesis, Technische Universiteit Eindhoven, Eindhoven, The Netherlands.

[12] Krolo, J., Nagode, A., Peko, I., Dumanić Labetić, I., 2026. Process Analysis, Characterization and Multi-Response Optimization of Double-Walled WAAM Aluminum Alloy Structures. Applied Sciences, 16 (5), 2250.

[13] BIKAR METALS GmbH. EN AW-1050A – World of Metals. https://my.bikar.com/en_US/products/300_021-300-021-2 (accessed 3 July 2026).

[14] Washington Alloy Company, 2020. 2319 Aluminum Welding Wire. U.S. Alloy Co., Charlotte, NC, USA.

[15] Kisić, N., 2022. Additive Manufacturing Based on the Robotic MIG/MAG Process of LDX2101 Duplex Stainless Steel. Master's Thesis, University of Split, Faculty of Electrical Engineering, Mechanical Engineering and Naval Architecture, Split.

[16] ABB, 2020. Product Specification – IRB 1600/1660. Document ID: 3HAC023604-001, Revision AM, ABB Robotics.

[17] ABB, 2019. Product Specification – Controller IRC5. Document ID: 3HAC047400-001, Revision U, ABB Robotics.

[18] Treutler, K., Wesling, V., 2021. The Current State of Research of Wire Arc Additive Manufacturing (WAAM): A Review. Applied Sciences, 11 (18), 8619.

[19] Jozić, S., Bajić, D., Celent, L., 2015. Application of Compressed Cold Air Cooling: Achieving Multiple Performance Characteristics in End Milling Process. Journal of Cleaner Production, 100, 325–332.